Shear Behavior of Adsorbed Poly(ethylene Oxide) Layers in Aqueous Media

Liraz Chai[†] and Jacob Klein*[,†,‡]

Department of Materials and Interfaces, Weizmann Institute of Science, Rehovot 76100, Israel, and Physical and Theoretical Chemistry Laboratory, Oxford University, South Parks Road, OXI, 3QZ, U.K.

Received June 19, 2007; Revised Manuscript Received September 26, 2007

ABSTRACT: We use a surface force balance to study shear interactions between adsorbed poly(ethylene oxide) layers (M_w = 150 000 or 170 000) adsorbed onto mica in 0.1 M KNO_3 aqueous solution. The shear forces increase with increasing compression of the layers or with increasing shear rates (at a constant compression), though at high compressions or shear rates the shear stress σ_s appears to saturate. This behavior is attributed to frictional effects that are dominated by viscous dissipation (and possible weak monomer−monomer complexing) between the mutually sliding layers at low compressions or shear rates, and by a substrate-slip mechanism at the highest compressions and shear rates. The shear behavior of adsorbed PEO layers in aqueous electrolyte at the higher compressions or shear rates can be well understood in terms of the attachment mechanism of PEO segments, via ion ligands to the charged substrate (as elucidated earlier, *J. Am. Chem. Soc.* **2005**, *127*, 1104).

Introduction

Poly(ethylene oxide) (PEO) is widely used in industry, technology and in scientific research for purposes ranging from stabilization or flocculation of colloidal dispersions[1,2] to control over ionic mobility in the solid phase[3,4] or in organic solvents.[5] PEO is unique for being nonionic and miscible in both organic solvents (such as toluene) as well as in water,[6] and in turn, it is compatible with both hydrophobic and hydrophilic surfaces. Being hydrophilic, it is often used in biological sciences, biotechnology, and pharmacology as an osmotic pressure modifier (and then it is often referred to as poly(ethylene glycol), PEG). Its biological applications include encapsulation of drugs for controlled release[7] or transport into tumor cells[8] and initiation of protein crystallization.[9,10] It is also grafted onto surfaces to prevent cell and protein adhesion,[11−15] and hence its binding mechanism onto surfaces as well as its friction behavior is important.

The properties of adsorbed and of end-grafted polymers, including PEO, have been extensively studied in recent decades using direct methods including reflectometry[16,17] and scattering[18,19] methods for probing the structure of the layers, and surface-force balance (SFB) approaches[20,21] for studying normal and shear interactions between the surface-attached polymer layers. The latter studies include neutral and charged polymers, and both adsorbed layers—where every monomer has a propensity to attach to the surface—and polymer brushes, where only the ends of otherwise-nonadsorbing chains are attached to the substrate surface.[22−36] Forces, in particular shear forces between surface-attached chains, can moreover differ markedly depending on whether the solvent is organic or an aqueous electrolyte, due to the polar nature of the water molecules and the presence of possible hydration layers that may provide lubrication.[26,32,37] It is of interest to examine the range of different cases that have been studied, as shown in Table 1. From this it can be seen that the one "missing" case concerns the shear behavior of adsorbed polymers in aqueous solvents and this provides part of the motivation for the present study. PEO, one of the few neutral (i.e., nonionizing) polymers that is water-soluble, has previously been used extensively as a model polymer for studying normal interactions in aqueous media[23,24,38] and shear interactions in organic media.[39] Studying the behavior of adsorbed PEO in aqueous media is therefore of interest, especially in view of the tendency of PEO chains to retain the etheric segments as chelating agents of alkali ions, with potassium in particular.[40] The recent demonstration[41] that the adsorption of the nonionic PEO onto a negatively charged mica surface (and most substrates tend to be charged under water) takes place, unusually, via an ion ligand rather than via van der Waals interactions, is a further manifestation of the different considerations in water relative to nonaqueous solvents.

Table 1. Summary of Some Studies on the Normal and Shear Forces between Surfaces Bearing Nonionic Polymers in Organic or Aqueous Environment

	aqueous		organic	
	normal	shear	normal	shear
adsorbed	23, 24, 41−43	this study	24, 39	39
brushes	25, 38, 44, 45	25, 37, 46, 47	22, 27, 28, 32, 34, 35, 48	22, 27, 32, 33, 49

In this paper we extend the earlier work on the adsorption of PEO onto mica in an aqueous environment,[23,41] and for the first time study the friction forces between such PEO layers. In particular, we compare our results with similar measurements on comparable PEO layers under the good organic solvent toluene, to obtain insight into the role of the different interaction forces in water.

Experimental Section

Materials. Tap water, passed twice through a reverse osmosis system, was subsequently passed through two polypropylene filters (of mesh size 25 μm and 2 μm) and a charcoal filter. The outcoming water was then treated with a three step Milli-Q system comprised of a reverse osmosis stage (RiOs), a UV treated reservoir and a Milli-Q Gradient A10 purification system. Using this cleaning procedure we obtained ultrapure (conductivity) water with 3−4 ppb of total organic compound (TOC as indicated by the A10 detector)

* Correspondence should be sent to the following email address: jacob.klein@weizmann.ac.il or jacob.klein@chem.ox.ac.uk.
[†] Department of Materials and Interfaces, Weizmann Institute of Science.
[‡] Physical and Theoretical Chemistry Laboratory, Oxford University.

10.1021/ma071352u CCC: $40.75
Published on Web 02/16/2008

and specific resistivity of at least 18.2 MΩ cm. The water pH was 5.5 (as measured with a Merck pH paper) due to dissolved CO_2 from the air.

Poly(ethylene oxide) of two molecular weights, $M = 150$K and 170K was purchased from Polymer Laboratories Ltd. and used as received. According to manufacturer's data, the end groups were t-butyl and hydroxyl and the polydispersity was $M_w/M_n = 1.02$. Aqueous solutions were prepared from potassium nitrate 99.999% that was purchased from Aldrich. After each use the salt was flushed with nitrogen and stored in a desiccator. The solvents used for cleaning were analytical grade ethanol, acetone and toluene. Ethanol was purchased from Merck and used after filtration with a 0.2 μm filter (type FG) from Millipore; acetone was purchased from J. T. Baker and toluene from Frutarom, Haifa, Israel. Sulfuric acid 95−98% from Palacid Ltd., and hydrogen peroxide 30%, chemically pure, from Frutarom, were used to prepare "piranha" solutions. Nitric acid 65% from Merck was diluted twice and used to clean stainless steel tools. Ruby muscovite mica, grade I, was supplied by S & J Trading Inc. (New York), and Epon 1004 resin from Shell was used to glue mica substrates onto fused silica lenses.

Methods. Prior to each experiment, all glassware were cleaned with a "piranha" solution (comprised of a 70:30 sulfuric acid: hydrogen peroxide mixture [***CAUTION!*** *piranha solution reacts violently with organic molecules and should be handled with extreme care]*). Thereafter the glassware and tools were washed with doubly deionized water and successively with ultrapure water taken from the Milli-Q system described above. All tools were then sonicated with toluene, ethanol and ultrapure water. Tools used for gluing were sonicated with acetone and ethanol prior to use.

We used a home-built surface force balance with the capability of measuring shear forces between the surfaces.[50] The surfaces used were back silvered mica pieces that had been melt-cut downstream of the laminar flow in a laminar flow hood by a platinum wire of 0.125 mm thickness and ca. 1 cm length. In order to ensure the cleanliness of the experiment, we first measured the contact position and shear forces in air. Then, we introduced water into the measuring cell and measured the force profiles and shear forces in water. In pure water the surfaces jump into an adhesive contact at a separation (-1 ± 0.5) nm relative to air (the result of removal in water of an air-adsorbed CO_2−water layer). Since this is the mica - mica contact it was set as the zero of contact throughout the rest of the experiment. Only following the jump-in in salt-free water did we exchange water with a 0.1 M KNO_3 solution. After measuring the force profiles in the salt solution we introduced PEO/0.1 M KNO_3, and measured force profiles following 12−16 h from the introduction of PEO solutions. PEO solutions were prepared at a concentration 150 μg/mL by dissolving the polymer in water and in 0.1 M KNO_3 solution at room temperature and stirring at 40 °C for 1−2 h, and were then allowed to cool to room-temperature prior to introduction into the SFB cell. Liquids were introduced into the SFB cell by opening the SFB in a laminar flow hood, separating the surfaces (to ca. 1 cm) and slowly pouring liquid solutions without using a syringe. This method of exchanging liquids reduces the accuracy of the absolute separation measurements from ±0.2−0.3 nm to ±0.5−0.6 nm, due to shifts in the optical fringe positions on repositioning the apparatus.

Shear force measurements were carried out in the usual way by mounting the top surface on top of a sectored piezo-electric tube (Pz 29 from Ferroperm, Denmark). Applying equal and opposite voltage to opposing sectors, a lateral motion ΔX_0 was applied to the top surface. The bending $\Delta X(t)$ of the shear spring in response to the shear forces transmitted between the surfaces was measured with an air-gap capacitor. Shear forces were then calculated from the displacement $\Delta X(t)$ as $F_s(D,t) = k_s \Delta X(t)$, with $k_s = 300$ N/m being the spring constant. The noise level in our measurements was ±2 μN. This was somewhat larger than in some earlier studies and was due to ambient vibrations that were not sufficiently compensated by the electronic vibration isolating system. The far field response was due to coupling arising from the thin wires connecting the Pz to the voltage supply. The signal-to-noise ratio could be greatly enhanced by carrying out a frequency analysis of the shear forces. By subtracting the large-separation noise level at the applied shear frequency from the measured shear forces between the compressed surfaces (at the same frequency), we were able to evaluate shear forces to ±60 nN within each experiment (statistical error from several contact positions). Results are shown from 5 different experiments with several different contact positions in each experiment. During an experiment the room was kept at a constant temperature (within ±0.5 °C) with temperature varying between 25 and 27 °C in different experiments.

Results

Normal Forces between PEO Layers in a 0.1 M KNO_3 Solution. In an earlier study,[41] we showed that although PEO does not adsorb onto mica from pure water, it does adsorb from 0.1 M KNO_3, in line with previous studies.[23] Normal surface interactions between PEO layers in 0.1 M KNO_3 on mica, following overnight incubation in 1.5×10^{-4} w/w PEO solution, are shown in Figure 1 together with surface interactions in 0.1 M KNO_3 (without added PEO). In 0.1 M KNO_3 the surface charge is screened by K^+ ions hence the interaction is short-ranged, with strong hydration repulsion at high compressions. From a best fit of the data in salt to the DLVO equation (solid line in the main figure) we extracted the surface potential in 0.1 M KNO_3, $\psi_0 = 90 \pm 30$ mV and the Debye screening length $\kappa^{-1} = 1.0 \pm 0.1$ nm. In contrast, across PEO layers in 0.1 M KNO_3, the onset of repulsion at $D \sim 80$ nm corresponds to the onset of overlap, $2L$, of the PEO chains, far beyond that in the absence of polymer. The extension from the surface, L (taken as half the onset of interactions), is some $3R_g$ (the radius of gyration $R_g \sim 13$ nm was taken from Klein et al.[23] where PEO of $M_w = 1.6 \times 10^5$ was used). At the onset of interaction, the tails of the polymer chains on each surface come into overlap, and the repulsion is due to the resulting osmotic pressure in the mid-plane, while at the highest compressions (smaller D values) the monomer-concentration in the gap becomes uniform and the osmotic repulsion is well-described by mean-field ideas.[23] The force−distance profiles agree well with previous normal force measurements between PEO layers adsorbed from 0.1 M KNO_3[23] (shown as the dotted line in Figure 1). Force profiles on withdrawal are generally shorter ranged than on approach (dashed line in Figure 1), as observed earlier for rapid decompression.[23]

By comparing the surface interactions across mica surfaces immersed in PEO/water solutions to those across PEO/0.1 M KNO_3, we were earlier able[41] to attribute the adsorption of PEO onto mica in 0.1 M KNO_3 to the binding of oxy−ethylene segments via hydrated or partly hydrated potassium cations, the latter serving as ligands to the negatively charged mica surface. The schematic in the inset to Figure 1 shows our proposed mechanism for the binding of the nonionic PEO segments onto the negatively charged mica.[41]

Shear Forces. Following the normal-force profile controls, we measured the shear force between the adsorbed PEO layers at decreasing D. The applied shear motion of amplitude ΔX_0 (shear velocity, $V_s = 180$ nm/s) together with the shear force transmitted to the bottom surface are shown in Figure 2 for decreasing D for typical shear traces. Following PEO adsorption, at separations larger than some $D = D_c$, there is no measurable shear coupling between the surfaces. This is shown by the frequency analysis of the shear force in trace b (RHS to trace b in Figure 2): at $D = 47.7$ nm, where the adsorbed PEO layers are already quite compressed, the shear force at the driving frequency (solid line) is similar to the larger-separation value ($D = 218$ nm, dotted line). At smaller separations, the motion

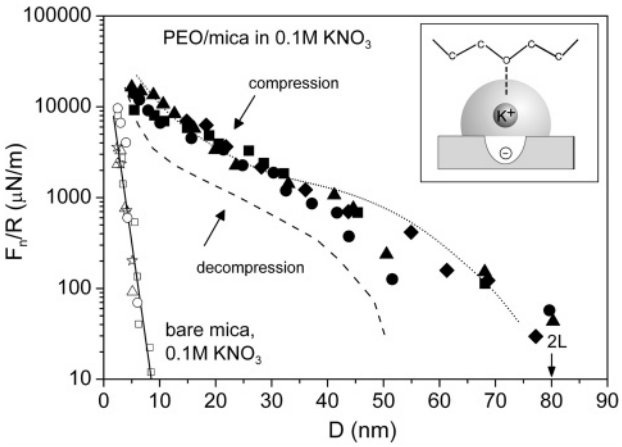

Figure 1. Normal surface interactions in 0.1 M KNO_3 between bare mica surfaces (open symbols) and between adsorbed PEO layers (solid symbols, surfaces approaching; dashed line, surfaces separating). The fit (solid line) to the DLVO equation[21,58] for the bare mica in 0.1 M KNO_3 data corresponds to a surface potential $\psi_0 = 90 \pm 30$ mV and a Debye screening length $\kappa^{-1} = 1.0 \pm 0.1$ nm (in line with literature values[21]). Literature data[23] for force profiles between PEO layers is given by the dotted line. The onset of the normal interactions at $D = 2L$, is marked by an arrow. Results are taken from different experiments and contact positions. The inset is a schematic illustration of the adsorption of a PEO segment to the negatively charged mica, attributed[41] to co-ordination bonds with hydrated potassium ions.

ΔX_0 applied to the top surface causes a lateral (i.e., shear or frictional) force above the noise level to be measured between the adsorbed layers as they move past each other. The traces corresponding to the shear force between the surfaces can be divided into two regimes, as shown by the magnification of trace (f) together with the applied triangular motion. Region 1−2 corresponds to bending of the shear springs. In all the traces c−f, the bending of the springs, ΔX_{1-2}, measured by the deflection of the bottom surface, is smaller than the applied shear motion, $\Delta X_{\text{bending}}$ in this region (1−2). This implies that only a fraction of the applied shear motion, $f_{\text{bending}} = \Delta X_{1-2}/\Delta X_{\text{bending}}$, is transferred to the bottom surface ($f_{\text{bending}} \cong 0.6$ and 0.9 for $D = 25.6$ nm and $D = 6.9$ nm, respectively) and that there is some sliding of the top surface relative to the bottom one even before the free sliding shown in the plateau region of each trace. This partial sliding clearly results in some distortive shear of the compressed PEO layers: When the consequent shear stress is large enough the surfaces slide freely (region 2−3, plateau in the traces). The free sliding appears to set on more abruptly at the higher compressions, and we return to this point in the discussion.

On the basis of such traces as in Figure 2, we extracted the shear force required for free sliding, F_s, transmitted to the bottom surface as a function of surface separation, and plotted F_s vs D in Figure 3. The measurements were performed at various shear velocities, as indicated in the figure caption. As seen in Figure 3, the shear forces begin to increase significantly in the range $D \cong 22-35$ nm, corresponding to compression ratios $\beta = 2L/D \sim 3.6-2.3$. This value is comparable with the compression ratio for which significant shear forces commence with adsorbed PEO in toluene[39] ($\beta \sim 4$) as well as with adsorbed telechelic PEO in 0.1 M KNO_3[29] ($\beta \sim 2.8$). In the inset, we converted the shear force, F_s, into shear stress, $\sigma_s = (F_s/A)$, in order to account for the increase in contact area, A, with the increase in the normal force. The area A may be evaluated from Hertzian contact mechanics,[51] as explained in the discussion.

Finally, we measured the shear force across adsorbed polymer layers at increasing shear velocity, V_s, at given surface separations, D, as shown in Figure 4 for $D = 14$ nm: A back and forth shear motion was applied to the top mica surface at velocities $6 < V_s < 1350$ nm/s, and the force transmitted to the bottom surface was measured. The shear force dependence on shear velocity is shown in Figure 5 at different D values (as indicated in the figure caption). Each set of data points corresponds to a given D value, and hence a given contact area A, which does not change as the shear velocity (or equivalently shear rate) varies. In the inset we have replotted the data as shear stress, $\sigma_s = F_s/A$ vs shear rate, $\dot{\gamma} = V_s/D$. At the lower shear rates, the shear force (or the related shear stress σ_s) increases quasi-linearly, where beyond certain crossover values $\dot{\gamma}_c$ of the shear rate, σ_s appears to saturate. We note that, as elaborated further in the Discussion section, the saturation level of the shear force—within significant scatter—remains within a relatively narrow band, over the range of compressions studied, even when converted to a shear stress (inset, marked by the dashed frame). This band is at a magnitude larger than the shear stress between highly compressed, adsorbed PEO layers in toluene[39] over a range of shear rates, shown as asterisks in Figure 5, inset).

We also carried out normal force measurements after a first approach, shearing and separation of the surfaces. The normal force profiles on a second approach following shear showed little difference to the first approach prior to shear. We believe this is because the net repulsion between the surfaces, particularly at the higher compressions, depends largely on the overall number of polymer segments in the gap at any D, via their osmotic pressure (this is broadly true though the detailed picture is more subtle, see, e.g., ref 53). This segment-number is unlikely to change drastically following shear, while the change in adsorbed layer structure due to the shear—e.g. temporary disruption of the polymer−mica bonds—is likely to have only a small effect on the overall segmental osmotic pressure (and hence on F_n).

Discussion

Normal Forces between Adsorbed PEO/0.1 M KNO_3. The normal force profiles (Figure 1) between the surfaces immersed in PEO/0.1 M KNO_3 solution are characteristic of those between adsorbed polymers on mica, whether in organic or aqueous solvents under good solvent conditions.[23,24,39] As shown in Figure 1, the double-layer repulsion is screened out at the high salt concentration (with Debye length $\kappa^{-1} = 1.0$ nm), and repulsion due to steric interactions starts when PEO chains start to overlap.

Earlier work showed that PEO adsorbs to mica from salt solutions by co-ordination bonds to potassium ions at the mica surface[41] (and not via van der Waals dispersion forces), as illustrated in the inset to Figure 1, in line with the known complexation of PEO with alkali metal ions in organic or aqueous solvents[40,42] (co-ordination bonds may also form between the adsorbed chains, forming a PEO network that is weakly "cross-linked" by K^+ ions). In order to examine the implications of this, and since it is important for understanding the shear forces as will be explained below, we compare in Table 2 the properties of the adsorbed PEO layer from this study with those for PEO adsorbed from the good organic solvent toluene,[39] where the primary adsorption mechanism is via van der Waals attraction of the segments to the substrate.

Table 2 shows that for similar PEO samples adsorbed from similar concentrations and a compareable "goodness" of solvent (i.e., segment−solvent interaction values, χ), there is both a smaller adsorbance of PEO onto mica from toluene relative to

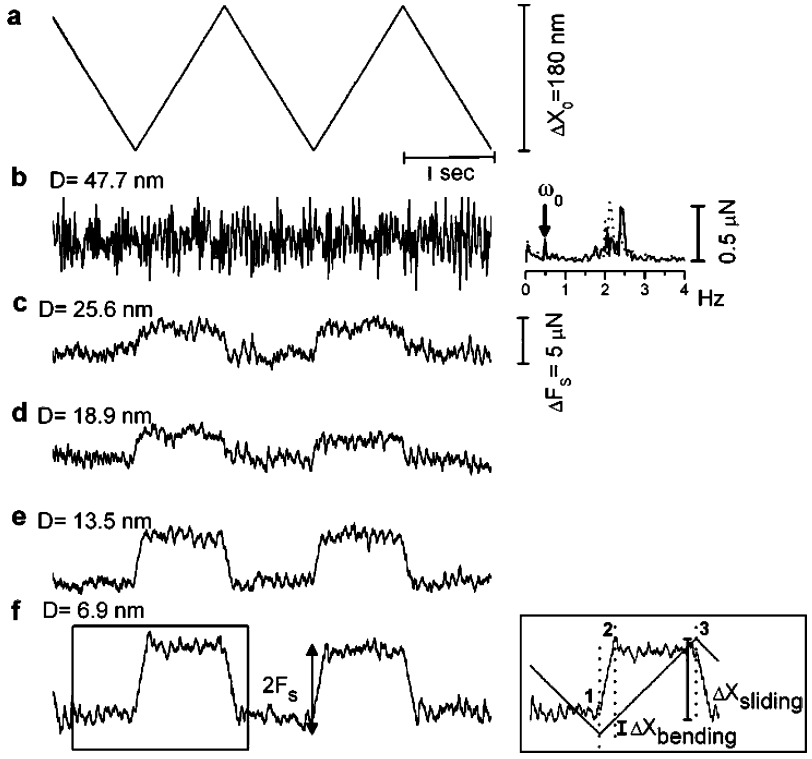

Figure 2. Shear forces between PEO layers in 0.1 M KNO_3 at decreasing D. (a) Back and forth shear motion, ΔX_0, applied to the top surface, with shear velocity $V_s = 180$ nm/s. (b - f) Shear force transmitted to the lower surface by the motion of the top one on approach (decreasing D). At very low compressions ($D = 47.7$ nm, trace (b)) the shear force at the driving frequency is similar to its value at larger separations as shown in the frequency analysis to the right (solid line: $D = 47.7$ nm, dotted line: $D = 218$ nm). At higher compressions (traces c−f), the shear force increases and two regimes can be identified (illustrated by the magnification of trace f, RHS), an increase in F_s (1−2) and a sliding regime (2−3), as discussed in the text.

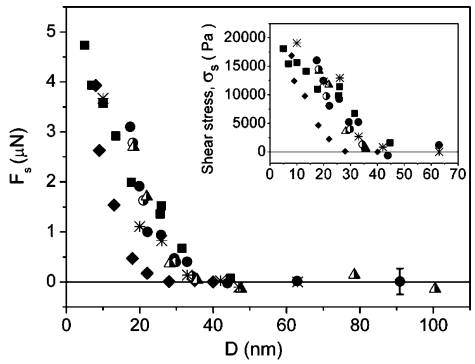

Figure 3. Shear force vs separation D across PEO layers in 0.1 M KNO_3 on a first approach. The measurements in the main figure were performed at different shear velocities: full symbols, $V_s = 150-180$ nm/s; half-filled symbols, $V_s = 36$ nm/s; asterisks, $V_s = 300$ nm/s. The inset shows the shear stress, $\sigma_s = F_s/A$, variation with D on a first approach. A is the contact area as was calculated[51] from the normal force−D plots in Figure 1, as explained in the discussion.

aqueous solutions, and at the same time a significantly more extended adsorbed layer (normalized in terms of R_g). We note however that the difference $(0.5 - \chi)$ is sensibly larger for PEO/toluene (0.11) than for PEO/0.1 M KNO_3 (0.02), suggesting better solvency conditions for the polymer in toluene. These features suggest a stronger segmental adsorption energy of PEO to mica from the 0.1 M KNO_3, via the K^+ ligands, relative to the adsorption from toluene which is presumably due to weaker van der Waals interactions. This very different type of bond with the charged mica surface can also be used to explain the other main features of our shear results.

Variation of Shear Forces with Compression. As seen in Figure 2 and summarized in Figure 3, the frictional forces between the PEO-bearing mica surfaces increase rapidly with compression once the shear force becomes measurable, in agreement with earlier observations for PEO adsorbed from toluene.[39] At lower compressions (e.g., trace c of Figure 2) the shear force appears to rise gradually to the sliding plateau value, suggestive of a viscous dissipation mechanism. At higher compressions the rise in the shear force F_s is a combination of bending of the shear springs (which increases the shear force) and sliding of the surfaces past each other. This is consistent with initial stretching of the chains when shear commences; the subsequent onset of sliding of the top surface when the shear force exceeds the friction force appears quite abrupt for these higher compressions (e.g., traces e, f in Figure 2). Normally, compression of adsorbed layers in good solvent increases both mutual entanglements and bridging,[23] which act to increase the frictional dissipation on shear. With confined PEO layers, overlapped chains may, as noted, also be part of a weak PEO network formed by PEO segments−K^+ complexation.[40] This qualitatively resembles weak cross-linking processes that could add to the increased dissipation on compression. However, the abrupt transition to sliding at the higher compressions suggests another mechanism, that was already earlier adduced both for polymer brushes[49] and for adsorbed chains in an organic solvent:[39] Namely, that when the shear force due to viscous dissipation within the sheared interpenetrated region of the overlapping chains becomes large enough, the slip plane shifts from the midplane to the polymer/substrate interface. We believe that this mechanism operates also in the adsorbed PEO/0.1 M KNO_3 system under study at the highest compressions, and we shall see that it is indeed capable of accounting for most of the features observed.

It is instructive to relate the variation of the shear force F_s required for sliding at a given surface separation D to the normal load F_n, thereby evaluating the effective friction coefficient

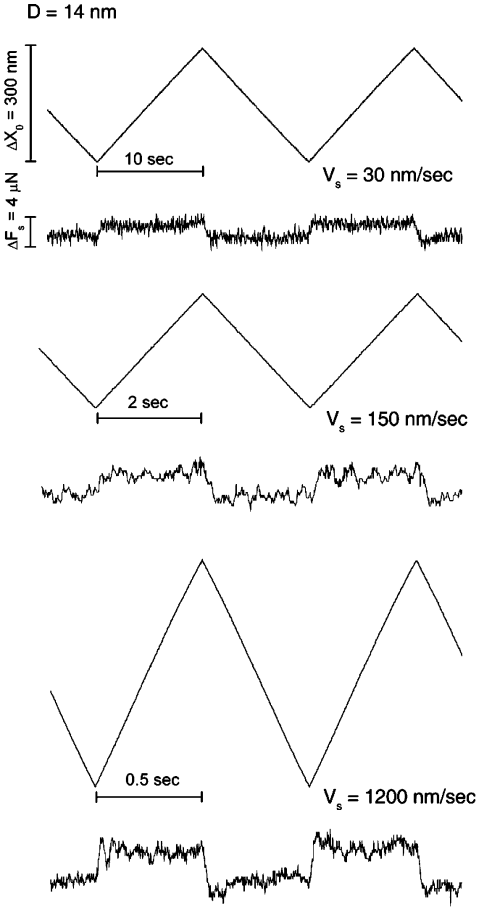

Figure 4. Shear forces between PEO layers in 0.1 M KNO_3 at various shear velocities, on first approach. Shear force (bottom traces), transmitted to the lower surface by the motion of the top surface (top, triangular motion) at varying velocities (from top to bottom, $V_s = 30$, 150, and 1200 nm/s). D was held constant at 14 ± 1 nm.

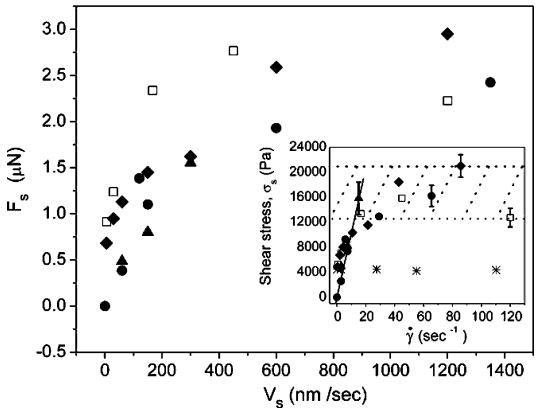

Figure 5. Dependence of shear force F_s on shear velocity. The plots were performed at shear velocities in the range 6 < Vs < 1350 nm/s and at different separations: (●) $D = 20.6$ nm, (▲) $D = 20$ nm, (◆) $D = 14$ nm, and (□) $D = 10$ nm. The data is replotted in the inset as shear stress, $\sigma_s = (F_s/A)$ vs shear rate, $\dot{\gamma} = V_s/D$, where A is the contact area between the surfaces. The solid line in the inset is a best fit to the linear variation regime. Asterisks (∗) correspond to data points from Figure 12 of ref 39 at $D = 11$ nm (and corresponding shear rates).

(defined as the ratio $\mu = F_s(D)/F_n(D)$) at that separation. The normal and shear forces vs D are therefore shown together in Figure 6 and the inset shows the friction coefficient, extracted from these plots, vs the compression ratio $\beta = 2L/D$. This plot shows that as D decreases, the shear forces are initially below the level of detection and therefore the effective friction coefficient must itself be rather low. This is probably due to

Table 2. Molecular Properties of PEO Adsorbed in Organic Solvent and in 0.1 M KNO_3

	PEO/0.1 M KNO_3[b]	PEO/toluene[39]
M_w (g/mol)	1.5×10^5 or 1.7×10^5	1.12×10^5
concentration (μg/mL)	150	100
R_g (nm)	13[a]	10.7
2L (in R_g units)	$6R_g$	$9R_g$
segment−solvent interaction parameter χ[24]	0.48	0.39
adsorbance, Γ, (mg/m^2)	2.8 ± 0.8 (this study, see following eq 1), 4.0 ± 1.5[23]	1.3 ± 0.3

[a] Taken from ref 23, where PEO of $M_w = 1.6 \times 10^5$ was used. [b] This study.

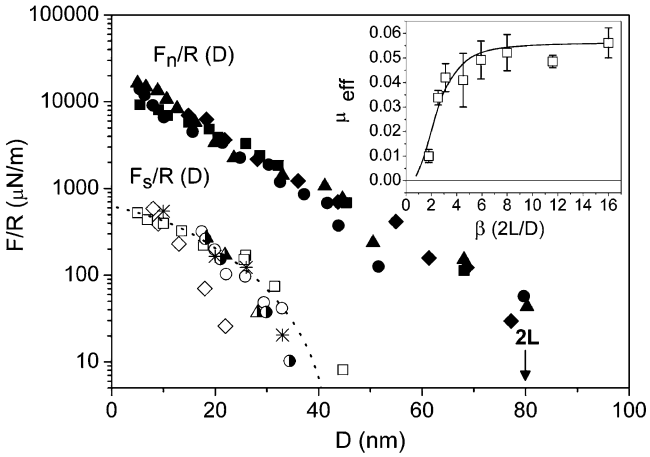

Figure 6. Normal and shear forces, F_n, F_s (normalized by the radius of curvature, R) vs separation D, taken from Figures 1 and 3. The dotted line is a guide to the eye for the $F_s(D)$/R data. The inset shows the friction coefficient, $\mu = F_s(D)/F_n(D)$, extracted from these plots, vs the compression ratio, $\beta = 2L/D$.

the same origin as for polymer brushes in good solvents: a fluid interface at low compressions which nonetheless correspond to a finite load between the surfaces, borne by the osmotic pressure of the overlapping segments at the midplane. At the higher compressions, in the region where F_s is measurable, relative growth of both normal and shear forces is observed, and it is reflected in the rise of μ with compression in the inset. The inset then reveals saturation of the friction coefficient at $\beta \sim 6$, which implies transition of the slip-plane from the polymer−polymer midplane to the polymer−surface interface.

The quantity which is of greater intrinsic physical interest, however, and provides a deeper insight into the frictional mechanism, is not the friction coefficient but rather the frictional *stress* σ_s when the surfaces slide past each other, given by $\sigma_s = (F_s/A)$, where A is the contact area between the sliding surfaces. The normal forces F_n increase due to the increase in the steric repulsion at higher compressions, but the shear forces should increase due to two different effects, namely the increase in mean monomer concentration in the gap (as $1/D$), together with the increased flattened contact area A resulting from distortion of the glue layers backing the mica sheets. The area A may be evaluated from Hertzian contact mechanics, and obeys[51] $A \cong \pi(F_nR/K)^{2/3}$, where $K \approx (1 \pm 0.3) \times 10^9$ N/m^2 is the effective modulus of the mica/glue combination.[50] It is of particular interest to examine how σ_s varies with the mean monomer volume fraction $\phi = (2\Gamma/\rho D)$ of the adsorbed chains (where Γ is the adsorbance and ρ is the monomer density, $\rho = 1.12$ gr/cm^3 for PEO). We may evaluate the adsorbance as follows: at sufficiently high compressions the interaction energy per unit area of flat plates $E(D)$, obeying the same force−distance law

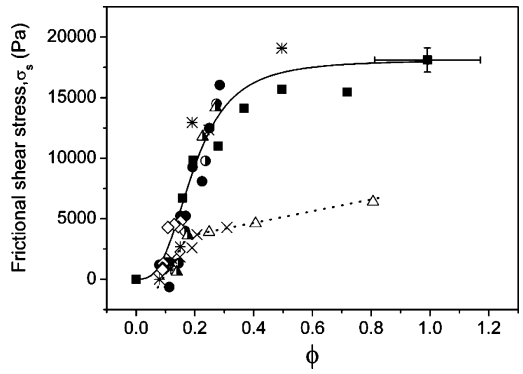

Figure 7. Frictional shear stress, $\sigma_s = F_s/A$, variation with the mean monomer volume fraction, $\phi = 2\Gamma/\rho D$ (Γ taken from Table 2 and the PEO density is $\rho = 1.12$ gr/cm^3): with PEO/0.1 M KNO_3 (to calculate σ_s we used normal and shear forces from Figures 1 and 3, respectively and the symbols correspond to those of Figure 3) and with PEO/toluene (normal and shear forces were taken from ref 39, Figures 4 and 8 respectively, with symbols corresponding to those from Figure 8; one exceptional data point from Figure 8 was omitted). Solid and dashed lines are used as a guide to the eye.

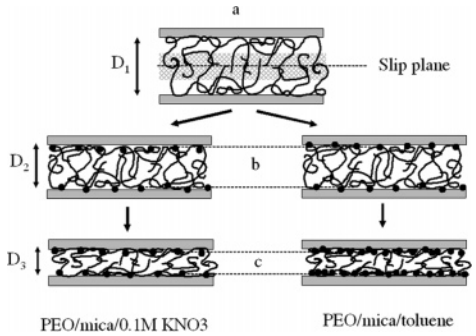

Figure 8. Schematic illustration of the proposed shear mechanism for the mica-adsorbed PEO, where $D_1 > D_2 > D_3$: (a) For both the aqueous (present study) and the toluene media, viscous dissipation takes place at low enough shear forces (weak compression or low shear rate) across the interfacial interpenetration region (cross-hatched). The slip plane is at the mid-plane, shown as a broken line. (b) At shear stresses beyond some value, the slip plane (broken lines) crosses over to the polymer/substrate interface, where the black circles (●) represent segment/mica attachments, either via ion−ligand binding (LH of part b, in 0.1 M KNO_3)) or van der Waals binding (RH of part b, in toluene). (c) At higher compressions the ion−ligand attachment density (LH of part c) remains unchanged as it is already saturated in part b, but more van der Waals attachments form in the toluene medium (RH of part c).

as the curved mica surfaces, $E(D) = F_n/2\pi R$ (Derjaguin approximation) is given by the following equation:[28]

$$E(D) \approx \text{const} \times \int_{D_1}^{D_2} \prod (\phi(D))\, \mathrm{d}D \approx \text{const} \times \left(\frac{2\Gamma}{\rho}\right)^2 \left[\frac{1}{D_2} - \frac{1}{D_1}\right] \quad (1)$$

where Π is the osmotic pressure ($\propto\phi^2$ in the mean-field limit, i.e., $\propto (1/D^2)$). In order to estimate Γ in our experiments, we used previous results[23] on PEO in 0.1 M KNO_3 to calculate the constant, as described for analogous cases earlier,[28] yielding $\Gamma = 2.8 \pm 0.8$ mg/m^2 (this value is consistent with the value $\Gamma = 4.0 \pm 1.5$ mg/m^2 determined in ref 23 for PEO of similar molecular weight in 0.1 M KNO_3).

Using these values of the adsorbance and of A, we can now plot the variation of the frictional shear stress σ_s with monomer volume fraction ϕ, and this is shown in Figure 7. We note that the value of σ_s for the higher compressions saturates with volume fraction at the highest compressions, i.e., the limiting frictional stress is, within the scatter, independent of the mean monomer concentration in the gap being sheared. This is a rather remarkable observation, since one would expect σ_s to increase with the monomer density, not only when the frictional dissipation is due to viscous shear of the polymer in the gap (where σ_s does increase with ϕ) but also, as we believe more likely at the highest compressions, when it is due to sliding of the polymer on the substrate. The origin of this surprising behavior—σ_s essentially independent of ϕ at high compressions—is, we believe, related to the ion−ligand mechanism by which the polymers adsorb onto the mica from 0.1 M KNO_3.[41] Such ligands form only at sites on the mica where K^+ ions have been lost to solution (there is, importantly, no net van der Waals attraction of PEO segments to the mica[41]), and the density of the sites on the surface is ca. 1/50 Å^2. If we assume a monomer size for the PEO of some 2−3 Å, then clearly a monomer volume fraction of 10−20% in the layer adjacent to the surface will suffice to saturate these ligand binding sites. Such a monomer surface concentration can readily exist even in the unperturbed adsorbed PEO layer (where the monomer concentration drops rapidly away from the surface,[52−54] and is certainly exceeded once the layers are mutually compressed. The implication is that at the point when, due to high compression, the slip plane shifts to the polymer/mica surface, the ion−ligand binding sites are already fully saturated, and further compression does not lead to any further attachment of the PEO to the surface. That is why the plateau shear stress (Figure 7) is essentially independent of further compression. It is instructive to compare this with the situation expected for PEO adsorbed to mica from toluene.[39] If our model is correct, then in the PEO/mica/toluene case—where van der Waals attraction is the main mechanism by which the PEO segments are adsorbed—the polymer/substrate sliding frictional stress should *increase* as the layers are compressed. This is because at the higher compressions more PEO segments would be forced into van der Waals adhesion to the mica surface, increasing the frictional stress when the layers are made to slide past the surface. In Figure 8, we sketch the expected situation in the two cases, PEO/mica/0.1 M KNO_3 (ion−ligand binding) and PEO/mica/toluene (van der Waals adhesion). In Figure 7 we have also plotted, from the data in ref 39, the variation of frictional stress σ_s with monomer volume fraction ϕ for the PEO/mica/toluene system. At low compression the shear stress shows a marked increase with ϕ corresponding to increased viscous dissipation, as for the PEO/mica/0.1 M KNO_3 case, but even at the higher compressions a clear (if small) increase is indicated up to the maximum ϕ attained in the toluene study, in line with our argument above and in contrast to the saturation (within scatter) of the shear stress for the present 0.1 M KNO_3 case.

Variation of Shear Forces with Shear Rate. The variation of shear forces F_s with shear rate $\dot{\gamma}$ shown in Figure 5 reveals that, at low values of $\dot{\gamma}$ and at moderately high compressions ($2L/D \approx 4-8$), F_s increases with the shear rate in a roughly linear, or Newtonian fashion $\sigma_s \propto \dot{\gamma}$ where as above $\sigma_s = F_s/A$ is the shear stress. This suggests that, at the lower values of shear rate, viscous shear within the gap is largely responsible for the frictional dissipation, since the alternative mechanism of sliding at the polymer/mica surface is likely to have a rather weak dependence on sliding velocity as observed earlier[39,49] and as a general observation for sliding friction at solid surfaces.[55] The precise details of how the compressed adsorbed layers are sheared when the surfaces slide past each other are complicated, as we cannot know precisely the extent of the region actually undergoing shear (indeed the extent of this region may decrease

with shear rate[27]). If nonetheless we make the assumption that the entire region of compressed adsorbed layers within the gap is undergoing shear when the surfaces slide, we may define an effective viscosity η_{eff} such that in the low shear rate regime:

$$\sigma_s = \eta_{eff}\dot{\gamma} \quad (2)$$

From a best fit of eq 2 to the plot in the linear (low $\dot{\gamma}$) part (Figure 5, inset), we may extract a value for the effective viscosity, $\eta_{eff} = 1000 \pm 100$ Pa s. This value is, interestingly, comparable to that expected from entangled bulk PEO solutions using the empirical relation[56] $\eta_{bulk} = (\text{const})\phi^5 M^{3.4}$: Putting η_{bulk} (5% water solution, $M = 2 \times 10^5$ PEO) = 0.055−0.095 Pa s,[57] we find η_{bulk} ($\phi = 0.35$, $M = 1.7 \times 10^5$) ≈ 0.5−1 kPa s.

At the higher shear rates shown in Figure 5 ($\dot{\gamma}_c >$ ca. 30 s^{-1}), the magnitude of the shear force (or shear stress) appears to saturate and become—within the scatter—only weakly dependent on $\dot{\gamma}$. This may be readily understood in terms of a shift to polymer/substrate sliding in similarity with the earlier discussion of saturation at increasing compression, though with a different mechanism whereby the shear stress increases with $\dot{\gamma}$ rather than with compression: As the shear force increases at higher shear rates, there comes a point (what we termed the critical shear rate $\dot{\gamma}_c$ when describing Figure 5) where the shear stress σ_s (eq 2) exceeds the yield stress at the polymer/mica interface, and the interface of weakest resistance to the shear shifts from the midplane to this (polymer/mica) interface.

Summary and Conclusions

We studied the shear properties of mutually compressed poly(ethylene oxide) layers adsorbed onto a solid charged surface (mica) from 0.1 M KNO_3 aqueous solution. The main difference in the adsorption behavior from an aqueous relative to an organic solvent arises from the ion−ligand attachment of the PEO chains to the mica surface from the aqueous electrolyte, as opposed to van der Waals adhesive attachment of PEO adsorbed from organic solvent. The long-ranged repulsion arising from steric interactions as two such adsorbed layers were compressed showed force profiles in line with literature behavior. The shear forces on sliding the surfaces past each other revealed that at low compressions or shear rates the frictional stress increased (with compression or shear rate), an effect attributed to viscous dissipation as the layers slid past each other across the midplane between them. At the highest shear rates or compressions the frictional stress saturated, reaching a value that, within the scatter, appeared essentially independent of both shear rate, and of compression (or equivalently, of the confined monomer volume fraction). This saturation is attributed to shift of the slip plane from the midplane to the polymer/mica interface. The unexpected independence of the limiting frictional stress from the confined monomer volume fraction is attributed to the fact that the ion−ligand attachment, by which PEO adsorbs, is saturated as the relatively few negatively charged surfaces sites are filled up by PEO attachment. Thus, further compression results in no additional surface attachment of the PEO, and therefore little additional shear stress as the adsorbed layers slide past the surface. In this the PEO/aqueous solution system differs qualitatively from the PEO/toluene one, where a weak but marked increase in the shear stress occurs at higher monomer volume fractions (higher compressions). In view of the ubiquity and importance of PEO in research and applications, this manifestation of its different surface behavior at a charged substrate, due to its unusual ion−ligand binding, may have interesting and widespread implications.

Acknowledgment. We thank Uri Raviv, Nir Kampf, and David Zbaida for helpful discussions and advice. This work was supported by the Israel Science Foundation, the Minerva Foundation, and the McCutchen foundation.

References and Notes

(1) Wang, D.; Yu, D.; Mo, M.; Liu, X.; Qian, Y. *J. Colloid Interface Sci.* **2003**, *261*, 565.
(2) Adachi, Y.; Wada, T. *J. Colloid Interface Sci.* **2000**, *229*, 148.
(3) Bruce, P. G.; Vincent, C. A. *J. Chem. Soc. Faraday Trans.* **1993**, *89*, 3187.
(4) Gray, F. M. *Solid Polymer Electrolytes: Fundamentals and Technological Applications*; VCH Publ,. Inc: New York, 1991.
(5) Belder, D.; Warnke, J. *Langmuir* **2001**, *17*, 4962.
(6) Brandrup, J.; Immergut, E. H.; Grulke, E. A. *Polymer Handbook*, 4th ed.; John Wiley & Sons, Inc.: New York 1999.
(7) Maggi, L.; Segale, L.; Torre, M.; Machiste, E.; Conte, U. *Biomaterials* **2002**, *23*, 1113.
(8) Mayhew, E.; Lasic, D.; Babbar, S.; Martin, E. *Int. J. Cancer* **1992**, *51*, 302.
(9) McPherson, A. *Crystallization of Biological Macromolecules*; Cold Spring Harbor Laboratory Press: Plainview: NY, 1999.
(10) Albertsson, P. A. *Partition of Cell Particles and Macromolecules*; Wiley: New York, 1986.
(11) Kenausis, G. L.; Voros, J.; Elbert, D. L.; Huang, N.; Hofer, R.; Ruiz-Taylor, L.; Textor, M.; Hubbell, J. A.; Spencer, N. D. *J. Phys. Chem. B* **2000**, *104*, 3298.
(12) Ryan, P. L.; Foty, R. A.; Kohn, J.; Steinberg, M. S. *P. Natl. Acad. Sci. U.S.A.* **2001**, *98*, 4323.
(13) Huang, N. P.; Michel, R.; Voros, J.; Textor, M.; Hofer, R.; Rossi, A.; Elbert, D. L.; Hubbell, J. A.; Spencer, N. D. *Langmuir* **2001**, *17*, 489.
(14) Roosjen, A.; Kaper, H. J.; vanderMei, H. C.; Norde, W.; Busscher, H. *Microbiology* **2003**, *149*, 3239.
(15) Pasche, S.; Voros, J.; Griesser, H. J.; Spencer, N. D.; Textor, M. *J. Phys. Chem. B* **2005**, *109*, 17545.
(16) Bijsterbosch, H. D.; Cohen, M. A.; Fleer, G. J. *Macromolecules* **1998**, *31*, 8981.
(17) Fick, J.; Steitz, R.; Leiner, V.; Tokumitsu, S.; Himmelhaus, M.; Grunze, M. *Langmuir* **2004**, *20*, 3848.
(18) Cosgrove, T.; Ryan, K. *Langmuir* **1990**, *6*, 136.
(19) Nelson, A.; Cosgrove, T. *Langmuir* **2004**, *20*, 2298.
(20) Tabor, D.; Winterton, R. H. *Nature (London)* **1968**, *219*, 1120.
(21) Israelachvili, J. N. *Intermolecular and Surface Forces*, 2nd ed.; Academic Press: London, 1992.
(22) Klein, J.; Kumacheva, E.; Perahia, D.; Mahalu, D.; Warburg, S. *Faraday Discuss.* **1994**, *98*, 173.
(23) Klein, J.; Luckham, P. F. *Macromolecules* **1984**, *17*, 1041.
(24) Luckham, P. F.; Klein, J. *Macromolecules* **1985**, *18*, 721.
(25) Raviv, U.; Frey, J.; Sack, R.; Laurat, P.; Tadmor, R.; Klein, J. *Langmuir* **2002**, *18*, 7482.
(26) Raviv, U.; Giasson, S.; Kampf, N.; Gohy, J.-F.; Jerome, R.; Klein, J. *Nature (London)* **2003**, *425*, 163.
(27) Tadmor, R.; Janik, J.; Klein, J. *Phys. Rev. Lett.* **2003**, *91*, 115503.
(28) Taunton, H. J.; Toprakcioglu, C.; Fetters, L. J.; Klein, J. *Macromolecules* **1990**, *23*, 571.
(29) Chestakova, A.; Lau, W.; Kumacheva, E. *Macromolecules* **2004**, *37*, 5047.
(30) Abraham, T.; Giasson, S.; Gohy, J. F.; Jerome, R. *Langmuir* **2000**, *16*, 4286.
(31) Kim, H. S.; Lau, W.; Kumacheva, E. *Macromolecules* **2000**, *33*, 4561.
(32) Schorr, P. A.; Kwan, T. C. B.; Kilbey, S. M., II; Shaqfeh, E. S.; Tirrell, M. *Macromolecules* **2003**, *36*, 389.
(33) Forster, A. M.; Mays, J. W.; Kilbey, S. M., II. *J. Polym. Sci., Part B: Polym. Phys.* **2006**, *44*, 649.
(34) Kilbey, S. M., II; Watanabe, H.; Tirrell, M. *Macromolecules* **2001**, *34*, 5249.
(35) Watanabe, H.; Tirrell, M. *Macromolecules* **1993**, *26*, 6455.
(36) Balastre, M.; Li, F.; Schorr, P.; Yang, J.; Mays, J. W.; Tirrell, M. *Macromolecules* **2002**, *35*, 9480.
(37) Muller, M. T.; Yan, X.; Lee, S.; Perry, S. S.; spencer, N. D. *Macromolecules* **2005**, *38*, 5706.
(38) Drobek, T.; Spencer, N. D.; Heuberger, M. *Macromolecules* **2005**, *38*, 5254.
(39) Raviv, U.; Tadmor, R.; Klein, J. *J. Phys. Chem. B* **2001**, *34*, 8125.
(40) *Nonionic surfactants*; Cross, J., Ed.; M. Dekker: New York, 1987; Vol. 19.
(41) Chai, L.; Klein, J. *J. Am. Chem. Soc.* **2005**, *127*, 1104. See also Chai, L.; Goldberg, R.; Kampf, N.; Klein, J. *Langmuir* **2008**, *24*, 1570.
(42) Kuhl, T. L.; Berman, A. D.; Hui, S. W.; Israelachvili, J. N. *Macromolecules* **1998**, *31*, 8258.

(43) Perez, E.; Proust, J. E. *J. Phys., Lett.* **1985**, *46*, L79.
(44) Heuberger, M.; Drobek, T.; Spencer, N. D. *Biophys. J.* **2005**, *88*, 495.
(45) Kuhl, T. L.; Leckband, D. E.; Lasic, D. D.; Israelachvili, J. N. *Biophys. J.* **1994**, *66*, 1479.
(46) Yan, X.; Perry, S. S.; Spencer, N. D.; Pasche, S.; Paul, S. M. D.; Textor, M.; Lim, M. S. *Langmuir* **2004**, *20*, 423.
(47) Zhang, X.; Granick, S. *Macromolecules* **2002**, *35*, 4017.
(48) Kumacheva, E.; Klein, J.; Pincus, P.; Fetters, L. J. *Macromolecules* **1993**, *26*, 6477.
(49) Klein, J.; Kumacheva, E.; Perahia, D.; Fetters, L. J. *Acta Polym.* **1998**, *46*, 617.
(50) Klein, J.; Kumacheva, E. *J. Chem. Phys.* **1998**, *108*, 6996.
(51) Johnson, K. L.; Kendall, K. K.; Roberts, A. D. *Proc. R. Soc. London, A* **1971**, *324*, 301.
(52) Fleer, G. J.; Cohen-Stuart, M. A.; Scheutjens, J. M. H. M.; Cosgrove, T.; Vincent, B. *Polymers at Interfaces*; Chapman and Hall: London, 1993.
(53) deGennes, P. G. *Macromolecules* **1981**, *14*, 1637.
(54) Cosgrove, T. *J. Chem. Soc. Faraday Trans.* **1990**, *86*, 1323.
(55) Bowden, F. P.; Tabor, D. *The Friction and Lubrication of Solids*; Clarendon Press: Oxford, U.K., 2001.
(56) Ferry, J. D. *Viscoelastic Properties of Polymers*, 2nd ed.; John Wiley & Sons, Inc.: New York, 1970.
(57) Bailey, F. E.; Koleske, J. V. *Poly(Ethylene Oxide)*; Academic Press: New York, 1976.
(58) Derjaguin, B. V.; Churaev, N. V.; Muller, V. M. *Surface Forces*; Consultants Bureau: New York, 1987.

MA071352U